Transition strengths and the role of the $f_{7/2}$ orbital in ^{71}As

R. A. Kaye,[1] C. J. Drover,[1] S. L. Tabor,[2] J. Döring,[3] Y.-C. Yang,[4] Y. Sun,[4] S. R. Arora,[1] N. R. Baker,[1] J. K. Bruckman,[5] T. A. Hinners,[2] C. R. Hoffman,[2,*] and S. Lee[2]

[1]*Department of Physics and Astronomy, Ohio Wesleyan University, Delaware, Ohio 43015, USA*
[2]*Department of Physics, Florida State University, Tallahassee, Florida 32306, USA*
[3]*Bundesamt für Strahlenschutz, D-10318 Berlin, Germany*
[4]*Department of Physics, Shanghai Jiao Tong University, Shanghai 200240, People's Republic of China*
[5]*Department of Physics, Monmouth College, Monmouth, Illinois 61462, USA*

(Received 15 December 2010; revised manuscript received 11 March 2011; published 25 April 2011)

High-spin states in ^{71}As were studied using the ^{54}Fe(^{23}Na,$\alpha 2p$) reaction at 80 MeV. Prompt γ-γ coincidences were measured using the Florida State University Compton-suppressed Ge array consisting of three clover detectors and seven single-crystal detectors. The existing high-spin level scheme has been verified, and 21 new transitions have been added based on an investigation of weak γ-ray coincidence relations and relative γ-ray intensities. Lifetimes of 16 excited states were measured using the Doppler-shift attenuation method applied to the experimental line shapes of decays in all of the known rotational bands. The $B(E2)$ strengths inferred from the lifetimes indicate that moderate to high collective behavior persists to the highest observed spins in the lowest positive- and negative-parity bands, in qualitative agreement with projected shell-model calculations. The band suggested to be based on the $\pi f_{7/2}$ orbital shows a similar degree of collectivity within the same spin range, with $B(E2)$ values in good agreement with those predicted by the projected shell model assuming a constant prolate deformation of $\epsilon_2 = +0.27$. The experimental Q_t values in this band are somewhat smaller than predicted by cranked Woods-Saxon calculations.

DOI: 10.1103/PhysRevC.83.044316 PACS number(s): 21.10.Tg, 23.20.Lv, 25.70.Hi, 27.50.+e

I. INTRODUCTION

Nuclei in the mass $A \approx 70$ region are well known to exhibit structural properties that vary sensitively with the number of protons (Z) and the number of neutrons (N). The valence space for both protons and neutrons in this region resides in the vicinity of large shell gaps in the Nilsson single-particle energy spectrum at different deformations and particle numbers [1], resulting in strong shape competitions and rapid shape changes with Z, N, and spin. These nuclei thus provide an excellent laboratory for studying the interplay between single-particle and collective degrees of freedom, especially when lifetime measurements are available to infer the degree of collectivity within structures based on different intrinsic configurations.

Previous studies of ^{71}As have revealed a richness of structure that has become a hallmark of nuclei in this region. In particular, a rather complex network of both collective and noncollective states has been observed and related to an associated evolution of competing shapes [2,3]. Despite this complexity, existing lifetime measurements [2] have made it possible to characterize the degree of collectivity and deformation of several excited states, and to more clearly interpret them in light of the predictions of a variety of theoretical approaches, including particle-rotor [4] and cranked Woods-Saxon [2] calculations. For example, lifetime measurements in the yrast positive-parity band of ^{71}As have helped illuminate the deformation-driving properties of the $g_{9/2}$ orbital and how the quasiparticle occupation of this orbital relates to the evolution of shape with spin [2,5,6].

Although the level schemes of the light odd-mass nuclei in this region show several similarities, one feature of the ^{71}As decay scheme that appears to be unique among its neighbors is the existence of a negative-parity band that is suggested to be based on the $[303]\frac{7}{2}^-$ prolate-deformed Nilsson configuration stemming from the $\pi f_{7/2}$ spherical orbital [3]. This interpretation was supported by the observation of relatively large $B(M1)/B(E2)$ ratios between 4 and $6\mu_N^2/(e\text{b})^2$ within this band, which agreed with the theoretical expectation if the states were based on an $f_{7/2}$, $K = \frac{7}{2}$ proton orbital with $g_s = 0.65 g_s^{(\text{free})}$, and assuming an average transition quadrupole moment $Q_t = 3.1\ e$b (corresponding to a prolate deformation of $\epsilon_2 = +0.37$) [3]. Thus far, however, the lifetimes of states in this band have not been measured to provide a means to test this prediction. The participation of the $f_{7/2}$ orbital in the structure of ^{71}As is intriguing, as it has already been shown to play a crucial role in the development of both superdeformed and strongly coupled, smoothly terminating bands in ^{62}Zn [7,8]. An extensive search was performed recently for a similar $f_{7/2}$ band in ^{69}As, but no clear candidate was found [9].

The present investigation was thus undertaken to measure as many lifetimes as possible in ^{71}As using the Doppler-shift attenuation method (DSAM) in order to quantify the degree of collectivity in the proposed $\pi[303]\frac{7}{2}^-$ structure, as well as to enhance the knowledge of the collective behavior in the yrast positive- and negative-parity bands at higher spin. An additional goal of this work was to carefully investigate weak

*Present address: Physics Division, Argonne National Laboratory, Argonne, IL 60439.

γ-ray coincidence relationships in an attempt to verify the band head of the $\pi[303]\frac{7}{2}^-$ structure and to look for transitions that link this structure to the low-spin levels known from the EC + β^+ decay of ^{71}Se [10].

II. EXPERIMENTAL AND ANALYSIS TECHNIQUES

High-spin states in ^{71}As were populated following the ^{54}Fe(^{23}Na,$\alpha 2p$) fusion-evaporation reaction at a beam energy of 80 MeV using the John D. Fox superconducting accelerator at Florida State University (FSU). In order to measure lifetimes using the DSAM, a thick 14 mg/cm^2 ^{54}Fe target was used to stop all recoiling nuclei. Prompt γ-ray coincidences, recorded within a time window of $\sim$100 ns, were detected using the FSU array of ten Compton-suppressed Ge detectors, consisting of three clover detectors placed at 90° relative to the beam direction, and single-crystal detectors placed at 35° (two detectors), 90° (two), and 145° (three). Approximately 4.6×10^8 total coincidence pairs were collected and sorted into a variety of γ-γ coincidence matrices with a dispersion of 0.7 keV/channel. Both the sorting and analysis of the γ-ray spectra were performed using GNUSCOPE, a γ-spectrum analysis software package developed at FSU [11,12].

The γ-ray coincidence relations that were used to both verify and enhance the existing level scheme were investigated mostly from background-subtracted spectra projected from matrices consisting of coincidences among the 90° detectors in order to minimize Doppler shifting. Doppler-shifted line shapes measured at 35° (145°), necessary for the DSAM lifetime analysis, were obtained from background-subtracted spectra projected from matrices consisting of coincidence events between 35° (145°) detectors and 90° detectors. Individual gates were set at 90° so that they encompassed the total extent of the chosen peak in the spectrum. Approximately 6.4×10^7 (9.2×10^7) coincidence pairs were collected in the 35° (145°) versus 90° detectors matrix.

The choice to analyze 35° and 145° spectra measured from coincidences with only the 90° detectors took advantage of the enhanced detection efficiency at 90° in the FSU array, and seemed to provide the best balance between sufficient statistics and line-shape purity, even allowing for Doppler broadening as necessary when gating. Alternative approaches to the analysis involve selective gating on portions of the line shape of a feeding [13] or depopulating [14,15] transition. However, these novel approaches would likely not have been beneficial in this case, given the observed difficulty to consistently obtain clean line shapes with sufficient statistics for a reliable lifetime measurement.

Mean lifetimes of excited states were then measured by applying the DSAM to the experimental line shapes of coincident γ rays detected at 35° and 145°. Theoretical line shapes were calculated using the simulation code FITS [16]. The nuclear and electronic stopping powers were obtained from the SRIM-2008 software [17].

By varying the lifetime of the parent state of interest, a set of theoretical line shapes was produced and compared with the measured Doppler-shifted spectrum at 35° and 145° to find the best fit. The lifetime which generated a curve that had the lowest χ^2 when compared to the experimental spectrum was taken as the lifetime of that state. The uncertainty in the individual lifetimes measured at both angles was determined by finding the lifetime value above and below the best-fit value which increased the minimum χ^2 value by one unit. The accepted lifetime values were determined from a weighted average (based on the measured uncertainty) of the individual lifetimes measured at both angles (see Table I). In some cases, this weighted average included contributions from a line-shape analysis of both an $M1/E2$ and a stretched $E2$ transition from the same initial state. The uncertainties in the accepted lifetimes were deduced from either the standard deviation of the set of individual lifetimes or the smallest uncertainty in the individual lifetime fits, whichever was larger.

Effective lifetimes, which do not include feeding corrections, were first determined from each line shape with adequate statistics. One effective lifetime representative of each state was determined from the weighted average (based on the individual uncertainties) of the results obtained from each of the two detector angles for which they could be measured. All line shapes were then refit with feeding corrections, with the exception of those from the highest fitted transition in each band, where only the upper-limit effective lifetime could be obtained. The feeding corrections used the effective lifetime of the state (or possibly multiple states) immediately above and one side-feeding state to feed the state of interest. The γ-ray intensities used in the feeding corrections, along with the γ-ray energies, were taken from Ref. [2] ([3]) for the positive-parity (negative-parity) states.

Whenever possible, mean lifetimes were determined from spectra gated from above (GFA) the transitions of interest, eliminating the effects of side feeding. However, limited statistics often required the analysis of line shapes obtained from spectra gated from below (GFB) the transition of interest. In these situations, the side-feeding times were assumed to follow a very similar model as was used in the most recent DSAM lifetime analysis for ^{71}As [2], since the lifetimes we obtained from a GFA analysis in general showed excellent agreement with the previous results which incorporated this side-feeding model for all measured lifetimes (see Sec. III B). This may be a consequence of the fact that the same compound nucleus (^{77}Rb) was produced at a similar maximum excitation energy as that of the reaction used in Ref. [2]. In this work, a side-feeding time of 0.04 ps was assumed for the $\frac{29}{2}^-$ state, the highest-lying one for which a mean lifetime could be extracted, and was assumed to increase by 0.03 ps per MeV of deexcitation. This choice is consistent with the assumptions used in other recent studies of nuclei in the mass 70–80 region (see, for example, Ref. [18]), which have been motivated by a rigorous theoretical study of side-feeding times in this mass region [19], as well as the measured results from ^{82}Sr [20] and ^{83}Y [21]. Of course, one should keep in mind that shorter (longer) side-feeding times used in the feeding corrections would result in longer (shorter) mean lifetimes. In many cases, however, the resulting mean lifetimes measured in this work were rather insensitive to the side-feeding time as long as the side-feeding intensity was small. In fact, an attempt to directly

TABLE I. Initial-state spins, γ-ray transition energies, mean lifetimes, electric quadrupole transition strengths $B(E2)$, magnetic dipole transition strengths $B(M1)$, and transition quadrupole moments $|Q_t|$ in ^{71}As. The level energies, transition energies, and spin assignments associated with previously known positive-parity (negative-parity) states were taken from Ref. [2] (Ref. [3]). Individual mean lifetimes deduced from a DSAM analysis of line shapes measured at the indicated angles from transitions with energy E_γ are given in the same row. The accepted mean lifetimes ($\tau_{\rm acc}$) represent the weighted average (based on the uncertainties) of the measurements at 35° and 145° where results are available.

I_i^π	E_γ (keV)	$\tau_{\rm prev}$ [a] (ps)	τ_{35° [b] (ps)	τ_{145° [b] (ps)	$\tau_{\rm acc}$ (ps)	$B(E2)$ (W.u.)[c]	$B(M1)$ (μ_N^2)[d]	$\lvert Q_t\rvert$ (eb)
				Band 1				
$\frac{13}{2}^+$	714.0	6.2(20)[e]			6.2(20)[e]	41^{+19}_{-10}		1.82^{+39}_{-24}
$\frac{17}{2}^+$	974.9	0.69(22)	0.76^{+73}_{-28}[f]		0.76^{+73}_{-28}[f]	70^{+41}_{-34}		2.13^{+55}_{-61}
$\frac{21}{2}^+$	1100.1	0.42(18)	0.42^{+16}_{-12}[f]		0.42^{+16}_{-12}[f]	69^{+28}_{-19}		2.02^{+37}_{-30}
$\frac{25}{2}^+$	1232.8	0.30(10)	0.33(5)	0.30^{+4}_{-3}	0.31^{+4}_{-3}	53(6)		1.72^{+9}_{-10}
$(\frac{29}{2}^+)$	1338.4		0.14^{+7}_{-5}	0.10(4)	0.12(4)	91^{+45}_{-23}		2.21^{+50}_{-30}
$(\frac{33}{2}^+)$	1447.4				<0.33[g]	>22		>1.08
				Band 3				
$\frac{15}{2}^-$	810.2		>2	>2	>2	<35		<1.58
	451.0						<0.15	
$\frac{19}{2}^-$	996.0			1.08^{+182}_{-50}	1.08^{+182}_{-50}	35^{+31}_{-22}		1.48^{+54}_{-58}
	626.4						0.04^{+4}_{-3}	
$(\frac{23}{2}^-)$	1156.9				<1.50[g]	>15		>0.93
				Band 4				
$\frac{13}{2}^-$	671.8	>2		>2[f]	>2[f]	<47		<1.96
	1075.4					<12		<0.98
$\frac{17}{2}^-$	820.6	1.86(33)	>2[f]	>2[f]	>2[f]	<59		<1.96
	369.6						<0.03	
$\frac{21}{2}^-$	943.4	0.85(23)		0.66^{+32}_{-17}[f]	0.66^{+32}_{-17}[f]	95^{+33}_{-31}		2.36^{+38}_{-42}
$\frac{25}{2}^-$	1137.5	0.33(12)	0.37^{+10}_{-8}	0.26^{+7}_{-6}	0.31(8)	79^{+28}_{-16}		2.10^{+34}_{-23}
$\frac{29}{2}^-$	1301.4	< 0.18	0.32^{+10}_{-9}	0.29(9)	0.30(9)	42^{+18}_{-10}		1.50^{+29}_{-18}
$\frac{33}{2}^-$	1442.0				<0.32[g]	>23		>1.11
				Band 6				
$\frac{15}{2}^-$	846.0		0.86^{+117}_{-35}	0.50^{+37}_{-20}	0.73^{+37}_{-20}	40^{+15}_{-14}		1.98^{+34}_{-37}
	442.6		0.92^{+38}_{-22}				0.66^{+25}_{-22}	
$\frac{19}{2}^-$	969.9				0.76(28)	36^{+21}_{-10}		1.61^{+42}_{-23}
	494.2		0.96^{+22}_{-15}	0.56^{+22}_{-15}			0.31^{+18}_{-8}	
$(\frac{23}{2}^-)$	1126.0				<0.54[g]	>39		>1.58
	584.6						>0.09	
				Band 7				
$\frac{13}{2}^-$	758.1		>2[f]		>2[f]	<20		<1.62
	403.5		1.40^{+222}_{-59}[f]	>2[f]			<0.34	
$\frac{17}{2}^-$	918.1				0.40(19)	52^{+47}_{-17}		2.06^{+78}_{-36}
	475.9		0.57^{+18}_{-13}	0.30^{+11}_{-10}			0.94^{+85}_{-30}	
$\frac{21}{2}^-$	1035.9				<0.83[g]	>22		>1.20
	541.6						>0.24	

[a] From Ref. [2] unless otherwise noted.
[b] Determined from spectra gated from below (GFB) the listed transition, unless otherwise noted.
[c] 1 W.u. = 17.46 e^2 fm^4.
[d] Assumes a dipole-quadrupole mixing ratio $\delta = 0$.
[e] From Ref. [6].
[f] Determined from spectra gated from above (GFA) the listed transition.
[g] Effective lifetime.

measure side-feeding times in ^{71}As through a comparison of GFA and GFB line-shape fits usually resulted in very large uncertainties, indicating an insensitivity of the observed GFB line shapes to the side-feeding time. Spin changes were measured for some of the newly observed transitions in ^{71}As based on directional correlation of oriented nuclei (DCO)

ratios, defined according to

$$R_{\rm DCO} = \frac{I_\gamma(\text{at } 35^\circ, 145^\circ;\ \text{gated by } \gamma_{\rm G} \text{ at } 90^\circ)}{I_\gamma(\text{at } 90^\circ;\ \text{gated by } \gamma_{\rm G} \text{ at } 35^\circ, 145^\circ)}. \quad (1)$$

In order to increase the statistics of the DCO ratio measurement, the analysis was performed using a matrix constructed to exploit the angular symmetry of the FSU Ge array, in which both 35° and 145° detector events were sorted against only the 90° detector events. Based on the geometry of the array, if the gate γ_G represents one or more stretched electric quadrupole ($E2$) transitions, then the DCO ratios for stretched $E2$ transitions as well as for $\Delta I = 0$ transitions are expected to be approximately unity, while $\Delta I = 1$ transitions yield ratios of about 0.5 if the mixing ratio is small [16]. DCO ratios for the new transitions were measured by gating on known stretched $E2$ decays [2,3]. All such measurable ratios are shown in Table II and reflect weighted averages (based on the measurement uncertainty) of the results obtained from two or more $E2$ gates.

III. RESULTS

A. ^{71}As level scheme

A partial level scheme of ^{71}As, relevant to the present work, is shown in Fig. 1. The most recent published level schemes [2,3] have been verified based on γ-γ coincidence relations, relative γ-ray intensities, and effective lifetime measurements. In addition to the band structures known from previous work, almost all of the non-yrast levels reported in Ref. [2] have been confirmed as well (but are not included in Fig. 1). The exception is the 1728.6-keV state, which the coincidence relations suggest does not exist. The 599.3-keV γ ray shown depopulating this state in Ref. [2] was instead determined to be a transition between the 2416.1- and 1816.7-keV levels based on the mutual coincidences observed between this transition and those at 687.4 and 821.2 keV, which would not be possible in the previous construction (see Fig. 5 in Ref. [2]).

Additionally, 21 new transitions have been assigned to ^{71}As based on a careful study of weak coincidence relationships. Some of these transitions, such as those at 858.8, 927.6, and 1492.2 keV, now clearly link some of the negative-parity high-spin states to low-lying states at 870.3 and 924.6 keV that were first established by a β-decay experiment [10] (see Fig. 1). Interestingly, three other new transitions of energy 329.9, 642.4, and 1467.8 keV imply a new state at 1467.8 keV that could be interpreted as the band head of the unfavored signature of the yrast negative-parity states (band 3 in Fig. 1). The measured DCO ratios of the 329.9- and 642.4-keV decays (see Table II) are consistent with $\Delta I = 1$ and $\Delta I = 2$ transitions, respectively, supporting a $\frac{7}{2}^-$ assignment for this state. The DCO ratio of 0.96(17) for the 1467.8-keV decay most likely implies a highly mixed transition. Figure 2 shows a portion of the background-corrected coincidence spectrum obtained by gating on the 996.0-keV transition, indicating the presence of the new 642.4- and 1467.8-keV lines.

Another goal of the search through weak coincidence relationships was to extend and enhance the high-spin portion of the ^{71}As level scheme as much as possible. In particular, a focused search was performed to extend the yrast positive-parity band (band 1 in Fig. 1) to as high a spin as possible since the first band crossing has yet to be observed there [2]. Although a 1447.4-keV transition was added at the top of this band, extending the sequence to a $(\frac{33}{2}^+)$ state at 7807.8 keV, this addition still does not provide clear evidence for the first quasineutron alignment (see Sec. IV A). However, two weakly populated high-spin structures (bands 2 and 5 in Fig. 1) have been added as side bands associated with the yrast negative-parity sequences (bands 3 and 4 in Fig. 1). The spin assignment of $\frac{21}{2}^{(-)}$ for the new state at 4571.4 keV was based on the measured DCO ratio of the 653.6-keV transition (see Table II), while the tentative assignments of other new states associated with band 2 assume $E2$ character for the intraband decays. The suggested spin assignments for the states in band 5 are primarily based on the measured DCO ratios for the two observed decays of the 3845.4-keV state, which indicate $\Delta I = 1$ ($\Delta I = 0$ or 2) character for the 554.8-keV (924.0-keV) transition and a resulting spin of either $I = \frac{15}{2}$ or $\frac{19}{2}$ for the 3845.4-keV state. However, a spin of $\frac{19}{2}$ is unlikely since the 3845.4-keV state is populated considerably less strongly than either of the other spin $\frac{19}{2}$ states shown in Fig. 1, thus favoring a spin of $\frac{15}{2}$. Negative parity is favored for both bands 2 and 5 since only linking transitions to known negative-parity states were observed. The observed coincidences between the 996.0-keV transition in band 3 and the 653.6-, 1011.3-, 1048.7-, 1197.8-, and 1211.0-keV transitions associated with band 2 are shown in Fig. 2.

TABLE II. Parent level energies, spin-parity assignments, γ-ray energies, DCO ratios ($R_{\rm DCO}$), and multipolarities (σL) associated with the new transitions assigned to ^{71}As in this work.

E_x (keV)	I_i^π	I_f^π	E_γ (keV)	$R_{\rm DCO}$	σL
1467.8	$\frac{7}{2}^-$	$\frac{5}{2}^-$	1467.8(4)	0.96(17)	$M1/E2$
1729.0	$\frac{7}{2}^-$	$\frac{5}{2}^-$	858.8(6)		$M1/E2$
1798.4	$\frac{9}{2}^-$	$\frac{7}{2}^-$	329.9(3)	0.56(25)	$M1/E2$
		$\frac{5}{2}^-$	927.6(2)	0.99(9)	$E2$
2111.0	$\frac{11}{2}^-$	$\frac{7}{2}^-$	642.4(2)	1.09(32)	$E2$
2417.0	$\frac{11}{2}^-$	$\frac{7}{2}^-$	687.7(2)		$E2$
		$\frac{7}{2}^-$	1492.2(5)		$E2$
2470.3	$\frac{13}{2}^-$	$\frac{13}{2}^+$	756.1(2)		$E1$
3845.4	$(\frac{15}{2}^-)$	$\frac{17}{2}^-$	554.8(4)	0.41(7)	$(M1/E2)$
		$\frac{15}{2}^-$	924.0(6)	0.82(41)	$(M1/E2)$
4571.4	$\frac{21}{2}^{(-)}$	$\frac{19}{2}^-$	653.6(3)	0.40(18)	$M1/E2$
4926.8	$(\frac{19}{2}^-)$	$\frac{21}{2}^-$	693.1(4)		$(M1/E2)$
		$(\frac{15}{2}^-)$	1081.1(4)		$(E2)$
5074.1	$(\frac{23}{2}^-)$	$\frac{21}{2}^-$	839.8(7)		$(M1/E2)$
5583.4	$(\frac{25}{2}^-)$	$(\frac{23}{2}^-)$	509.4(6)		$(M1/E2)$
		$\frac{21}{2}^{(-)}$	1011.3(4)		$(E2)$
		$\frac{21}{2}^-$	1211.0(6)		$(E2)$
6174.0	$(\frac{23}{2}^-)$	$(\frac{19}{2}^-)$	1247.2(11)		$(E2)$
6781.2	$(\frac{29}{2}^-)$	$(\frac{25}{2}^-)$	1197.8(5)	0.95(35)	$E2$
7807.8	$(\frac{33}{2}^+)$	$(\frac{29}{2}^+)$	1447.4(10)		$(E2)$
7829.9		$(\frac{29}{2}^-)$	1048.7(7)		

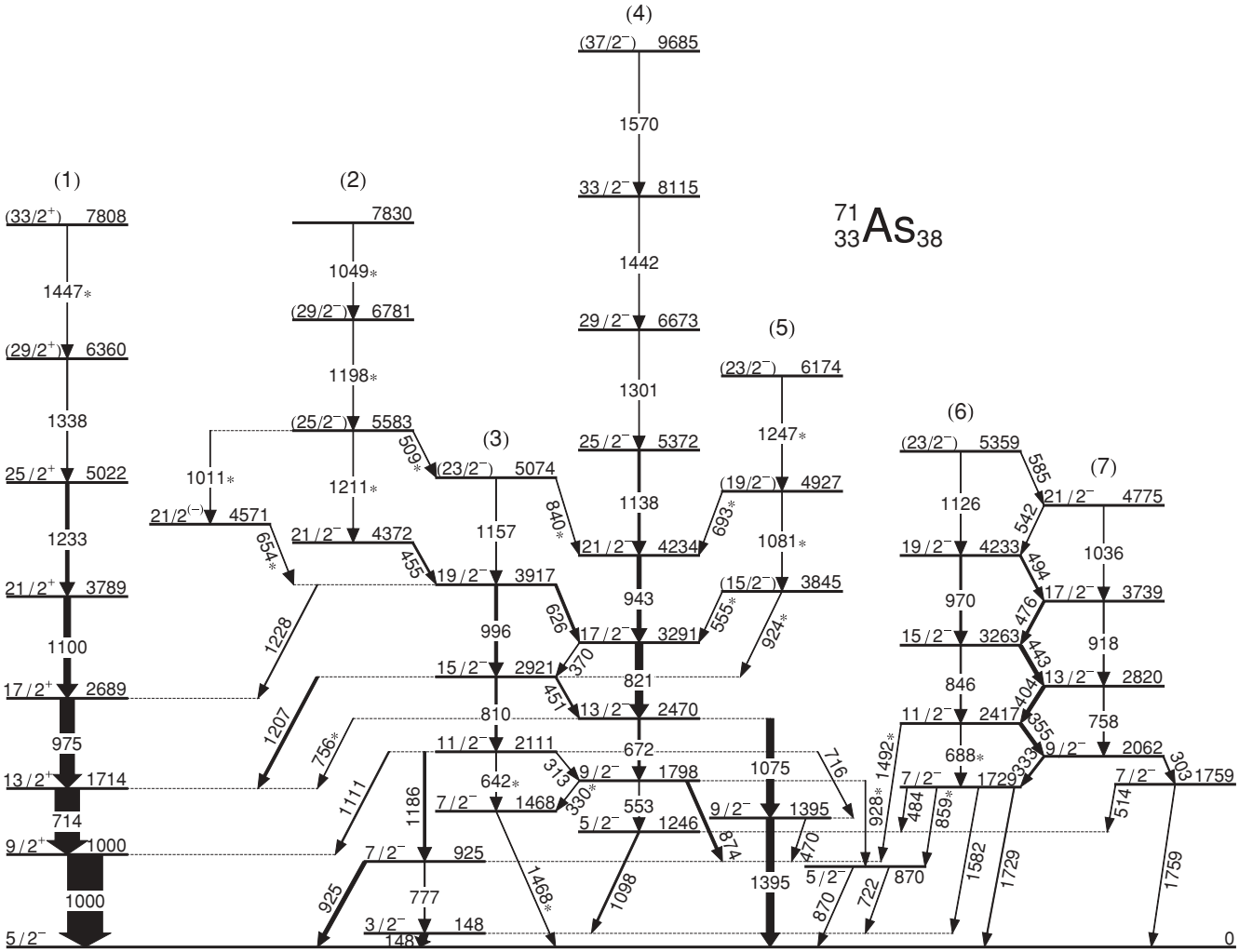

FIG. 1. Partial level scheme of ^{71}As relevant to the present work. Transitions introduced in this work are indicated with asterisks. The energies and decay intensities of all other transitions originating from positive-parity (negative-parity) states were taken from Ref. [2] ([3]). The arbitrary labels above each decay sequence are included to facilitate the discussion in the text.

B. Lifetime measurements

Lifetimes of 16 excited states were measured using the DSAM and are given in Table I. Mean lifetimes τ are given for each detector angle along with the accepted lifetime $\tau_{\rm acc}$ of each state which represents the weighted average of the results at each angle. Some of the values in the table indicate upper or lower limits on τ. Upper limits indicate effective lifetimes for which feeding corrections are either unavailable or unreliable due to limited statistics. Lower limits of 2 ps were placed on τ if the fits to the line shapes of the associated parent-state decays resulted in a χ^2 value that did not converge to a minimum below $\tau = 2$ ps when invoking feeding corrections. If a reliable line shape for a given transition could not be obtained at either 35° or 145°, a lifetime result at that angle is not included in the table. Results obtained from a previous DSAM analysis [2] are also included in Table I for comparison ($\tau_{\rm prev}$).

Two new lifetimes were measured in the yrast positive-parity band (band 1 in Fig. 1), including an upper-limit effective lifetime for the new $(\frac{33}{2}^+)$ state. As a check for possible systematic error and to develop a consistent model for side feeding (see Sec. II), the lifetimes of three other states reported in Ref. [2] were remeasured and found to be in excellent agreement (see Table I). In particular, the lifetimes of the $\frac{17}{2}^+$ and $\frac{21}{2}^+$ states were both determined from spectra that resulted from summing gates on the higher-lying 1232.8- and 1338.4-keV transitions. This not only eliminated the effects of unknown side feeding, but it also eliminated the need to correct for direct feeding from the 974.7-keV decay of a relatively long-lived $\frac{21}{2}^{(-)}$ state [2] (not shown in Fig. 1). Figure 3 shows three representative fits to the line shapes of transitions in this band measured at 35°.

Lifetime measurements were extended up to the $\frac{33}{2}^-$ state in the signature $\alpha = +\frac{1}{2}$ sequence of the yrast negative-parity states (band 4 in Fig. 1), where an effective lifetime has been measured. Of the lifetimes previously measured for this band [2], only the result for the $\frac{29}{2}^-$ state, < 0.18 ps, disagrees with our measurement within the range of experimental uncertainty (see Table I). The upper limit had been deduced from a single

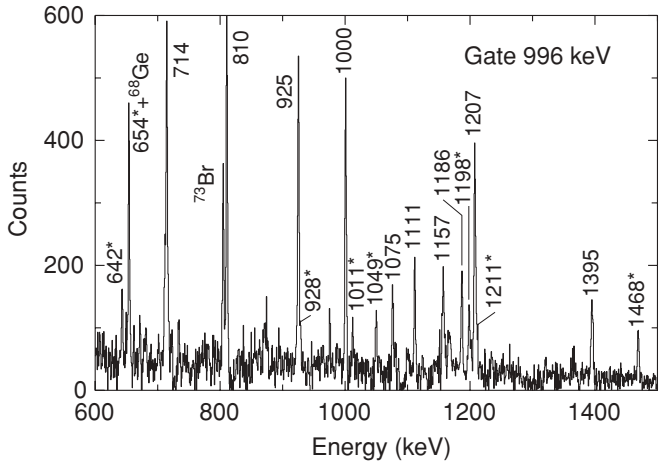

FIG. 2. A portion of the background-corrected coincidence spectrum obtained by gating on the 996.0-keV transition as measured by the 90° detectors. Peak energies labeled with asterisks indicate transitions assigned to ^{71}As in this work.

measurement in the forward direction only. In the current work, two separate values have been obtained from a line-shape analysis of the 1301.4-keV transition at both forward and backward directions with somewhat improved statistics compared to the previous measurement. Thus, the weighted average of the current results has been taken as the accepted lifetime for this state. Figure 4 shows the GFA fit to the line shape of the 943.4-keV transition ($\frac{21}{2}^- \rightarrow \frac{17}{2}^-$) in this band measured at 145°. In addition, three lifetime measurements were performed in the unfavored $\alpha = -\frac{1}{2}$ sequence (band 3 in Fig. 1) for the first time, although only an upper (lower) limit could be established for the ($\frac{23}{2}^-$) ($\frac{15}{2}^-$) state.

Lifetimes were measured in bands 6 and 7 (see Fig. 1) for the first time. Effective lifetime limits were placed on the highest observed states, and a lower limit of 2 ps was placed on the lifetime of the $\frac{13}{2}^-$ state from a GFA analysis, which indicated no observable Doppler shift for either the 403.5- or the 758.1-keV decays from this state. In general, the stronger $M1$ decays within this band provided more reliable line shapes than the weaker $E2$ decays from the same state, even though their smaller transition energies resulted in Doppler-shifted components that were closer in energy to the unshifted ones. Fits to the 35° line shapes of the 442.6- and 475.9-keV $M1$ transitions between bands 6 and 7 are shown in Fig. 4.

Reduced electric quadrupole transition strengths $B(E2)$ were determined for relevant $E2$ transitions from the accepted lifetime of the associated parent state, and were used to calculate transition quadrupole moments $|Q_t|$ from the rotational model according to

$$Q_t^2 = \frac{16\pi}{5}\langle I\,K\,20|I-2K\rangle^{-2}B(E2, I \rightarrow I-2). \qquad (2)$$

A spin projection quantum number of $K = \frac{5}{2}$ ($\frac{7}{2}$) was used to determine the $|Q_t|$ values for bands 1, 3, and 4 (6 and 7).

The Q_t values provide a measure of the quadrupole deformation β_2. For the purpose of discussion, some β_2 values have been calculated when it was appropriate to approximate

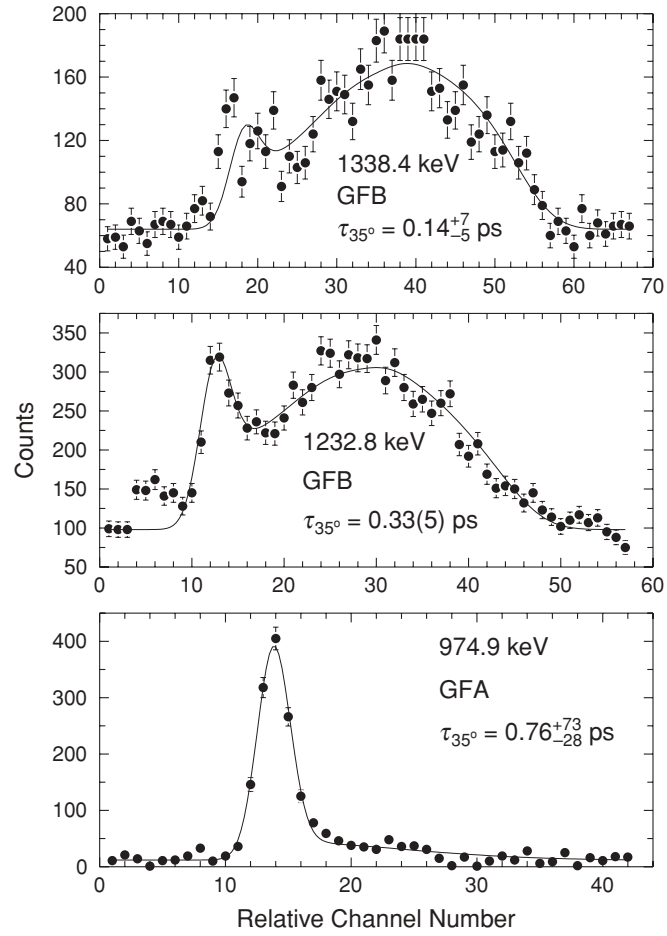

FIG. 3. Representative fits to the 35° line shapes of transitions belonging to band 1 in ^{71}As. Spectra obtained by gating from above (GFA) or gating from below (GFB) the transition of interest are indicated. Some error bars are smaller than the symbol size.

the nuclear shape as axially symmetric. In this case, β_2 is determined approximately by

$$|\beta_2| = \sqrt{\frac{49\pi}{80} + \frac{7\pi\,Q_t}{6eZr_0^2A^{2/3}}} - \sqrt{\frac{49\pi}{80}}, \qquad (3)$$

where $r_0 = 1.2$ fm was used. The $B(E2)$ and Q_t values inferred from the lifetime measurements are given in Table I.

Magnetic dipole transition strengths $B(M1)$ were estimated for $M1$ transitions associated with bands 3, 4, 6, and 7 in Fig. 1 assuming a dipole-quadrupole mixing ratio of $\delta = 0$ since $B(M1)$ values are rather insensitive to δ as long as it is small. At any rate, these $B(M1)$ estimates could be considered upper limits for these transitions. All deduced $B(M1)$ strengths are included in Table I.

IV. DISCUSSION

Of particular interest to this study is the high-K band structure based on relatively strong $\Delta I = 1$ transitions that develop above the $\frac{7}{2}^-$ state at 1729.0 keV (bands 6 and 7 in Fig. 1), since this feature has not been observed in

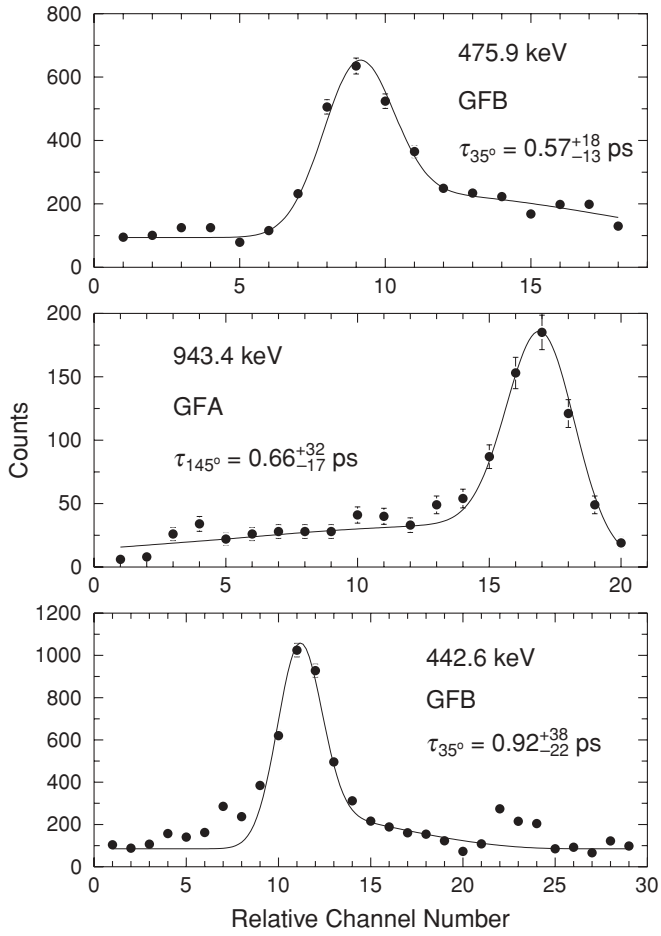

FIG. 4. Representative fits to the 35° or 145° line shapes of transitions between negative-parity states in ^{71}As. Spectra obtained by gating from above (GFA) or gating from below (GFB) the transition of interest are indicated. Some error bars are smaller than the symbol size. The contaminant in the shifted portion of the line shape of the 442.6-keV transition (bottom panel) was not included when performing the fit.

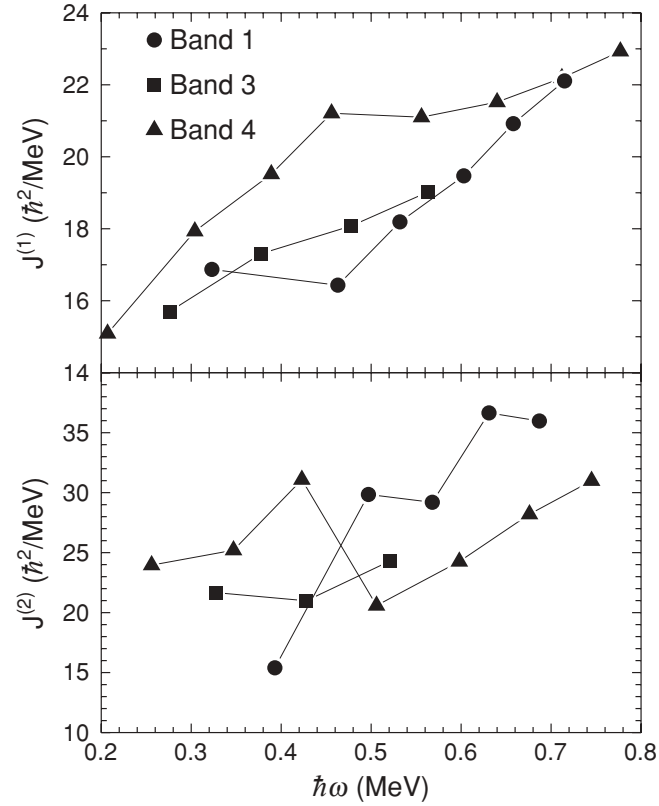

FIG. 5. Kinematic ($J^{(1)}$) and dynamic ($J^{(2)}$) moments of inertia as a function of rotational frequency $\hbar\omega$ for bands 1, 3, and 4 in ^{71}As. A common value of $K = \frac{5}{2}$ was used for all bands.

any other light, odd-mass isotope in the $A \approx 70$ region. So far, its interpretation as a strongly deformed rotational band based on an intrinsic $[303]\frac{7}{2}^-$ quasiproton configuration results from a comparison of experimental $B(M1)/B(E2)$ ratios with theoretical expectations that assume a quasiproton occupation of this orbital at a prolate deformation of $\epsilon_2 = +0.37$ [3].

Now that lifetime measurements are available for the first time in bands 6 and 7, the existing interpretation of these sequences has been reinvestigated using the projected shell model (PSM) through a comparison of measured and predicted $M1$ and $E2$ transition strengths. Further evidence for the nature of these structures was sought through cranked Woods-Saxon (CWS) calculations for non-yrast configurations. Additionally, lifetime measurements have been extended to higher spin in the yrast positive- and negative-parity states, so the high-spin collective properties of these bands have been revisited with the PSM as well. The implications of the new low-spin extension of band 3 (see Sec. III A) and the possible onset of the first quasineutron alignment in band 1 were also explored using the cranked shell model (CSM). The results of each of these investigations are discussed separately in the sections that follow.

A. Cranked shell-model calculations

The kinematic ($J^{(1)}$) and dynamic ($J^{(2)}$) moments of inertia as a function of rotational frequency were extracted for bands 1, 3, and 4 in ^{71}As using the CSM, and are shown in Fig. 5. A common value of $K = \frac{5}{2}$ was used for these bands, which is consistent with previous CSM calculations for these sequences [2].

As shown in the top panel of Fig. 5, the suggested low-spin extension of band 3, which includes the new 642.4-keV $E2$ transition, appears to fit the existing $J^{(1)}$ spectrum established by the other members of this band quite well. In a similar fashion, the known 552.6-keV transition between the 1798.4- and 1245.5-keV states [3] also seems to closely follow the established progression down to lower frequencies in band 4. Thus the $\frac{7}{2}^-$ state at 1467.8 keV ($\frac{5}{2}^-$ state at 1245.5 keV) could be interpreted as the band head of band 3 (4).

Figure 5 also shows that the placement of one additional transition above the established decays in band 1 [2] simply continues the nearly constant upward trend in $J^{(1)}$ without evidence of an alignment. Similarly, the $J^{(2)}$ moments of inertia associated with this band, which are sensitive indicators

of changes in $J^{(1)}$, show no indication of a peak and therefore an associated band crossing.

B. Projected shell-model calculations

Calculations have been performed within the context of the PSM [22] in order to further investigate the collective properties of the observed band structures in ^{71}As and their relationship to the intrinsic configurations involved. The PSM uses a rotational-invariant Hamiltonian including quadrupole-quadrupole, monopole-pairing, and quadrupole-pairing interaction terms. The strength of the quadrupole-quadrupole force was chosen so that the self-consistent relation with the input deformation parameter is kept. The monopole-pairing force strength took the form

$$G_M = \left[G_1 - G_2 \frac{N-Z}{A}\right] A^{-1}, \tag{4}$$

where $G_1 = 20.25$ for both neutrons and protons, and $G_2 = 16.20$ (0) for neutrons (protons). The quadrupole-pairing strength, assumed to be proportional to the monopole strength, was 16% of the monopole-pairing strength. These strengths are the same as those employed in previous PSM calculations for this mass region [23–26].

In the calculations, the deformed quasiparticle (qp) basis is constructed from the Nilsson single-particle states followed by a BCS calculation. The single-particle space includes all nucleons in the $n = 2, 3, 4$ major shells. To build the shell-model basis for a nucleus with an odd number of protons, the quasiproton creation operator is applied to the qp-vacuum state, and the resulting set of 1-qp states are projected onto good angular momentum states. The one-quasiproton states include, among others, the $[440]\frac{1}{2}^+$, $[310]\frac{1}{2}^-$, $[312]\frac{3}{2}^-$, and $[303]\frac{7}{2}^-$ orbitals which lie near the Fermi level for prolate deformations. In addition, the shell-model basis includes projected 3-qp states which are built by these one-quasiproton states plus a $g_{9/2}$ neutron pair. We expect that mixing of the configurations with 1-qp and 3-qp states at appropriate spins describes the rotation alignment of $g_{9/2}$ neutrons. The projected basis is used to diagonalize the shell-model Hamiltonian. The resulting eigenstates (wave functions) are then used to determine transition strengths [27]. The construction of shell-model basis states for odd-mass nuclei are restricted to the assumption of axial symmetry, so a fixed deformation parameter of $\epsilon_2 = +0.27$ (corresponding to prolate deformation) was used in order to achieve the best overall agreement with the experimental results for ^{71}As. In the $B(E2)$ calculation, standard effective charges of $e^\pi = 1.5e$ and $e^\nu = 0.5e$ were used. In the $B(M1)$ calculation, the free-nucleon values of $g_s^\pi = 5.586$ and $g_s^\nu = -3.826$ were damped by a usual 0.75 factor to account for the core-polarization and meson-exchange current corrections. The same values have been used for the determination of g factors in previous PSM calculations, without any adjustment for individual nuclei.

The $B(E2)$ strengths calculated by the PSM for the multiple band structures in ^{71}As are compared with the experimental ones deduced from the available lifetime measurements in Fig. 6. In general, the assumption of prolate symmetry

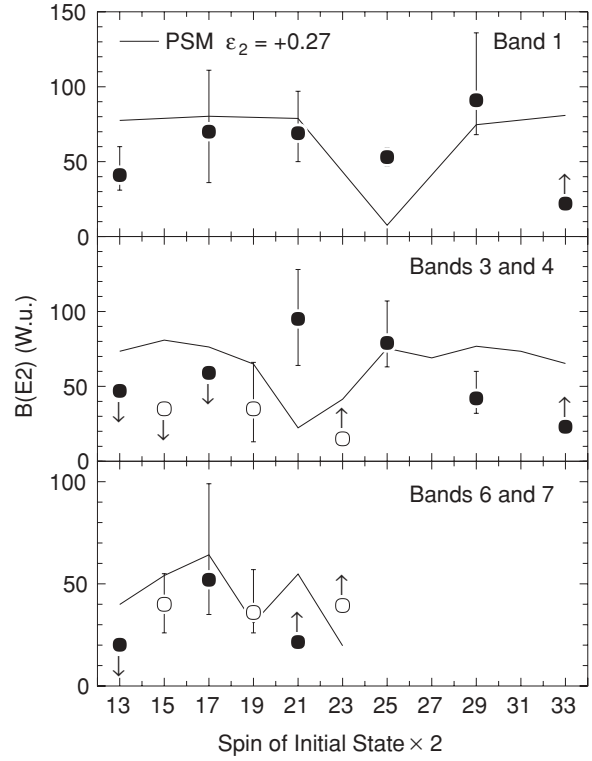

FIG. 6. $B(E2)$ strengths as a function of the initial-state spin for band 1 (top panel), bands 3 and 4 (middle), and bands 6 and 7 (bottom) in ^{71}As. Filled (open) circles indicate experimental values associated with a signature $\alpha = +\frac{1}{2}$ $(-\frac{1}{2})$ sequence. Symbols with arrows indicate either upper or lower limits established by the lifetime measurements, and one experimental value (corresponding to an initial state of $\frac{25}{2}^+$ in band 1) has error bars that are smaller than the symbol size. The solid curves represent theoretical predictions from projected shell-model calculations.

in the PSM calculations appears reasonable, especially for reproducing the $B(E2)$ values in bands 6 and 7 (lower panel in Fig. 6), where good agreement is obtained with the experimental results. Since quasiproton occupation of the $[303]\frac{7}{2}^-$ Nilsson orbital at prolate deformation was used for this calculation, this agreement strongly favors the $\pi f_{7/2}$ extruder configuration for these bands, in agreement with the interpretation of Ref. [3].

The predicted and measured $B(E2)$ values show much less agreement within bands 1, 3, and 4, as indicated in the top two panels of Fig. 6. However, the observed qualitative trends in band 1 appear to be at least roughly reproduced by the PSM calculations. The differences between the experimental and PSM results might be due to the lack of a triaxial degree of freedom in the PSM calculations, since triaxial shapes were shown to be important in describing the high-spin characteristics of these bands from total Routhian surface calculations [2], and additionally through the results of particle-rotor calculations for band 1 [4].

Magnetic dipole transition strengths $B(M1)$, which are sensitive to the single-particle attributes of the nuclear wave function, were also predicted for bands 6 and 7 from PSM calculations. The results are shown in Fig. 7, which

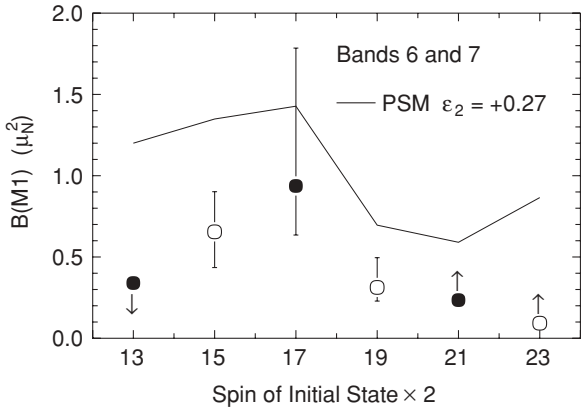

FIG. 7. $B(M1)$ strengths as a function of the initial-state spin for the $M1$ transitions between bands 6 and 7 in ^{71}As. Filled (open) circles indicate experimental values associated with a signature $\alpha = +\frac{1}{2}$ $(-\frac{1}{2})$ sequence. Symbols with arrows indicate either upper or lower limits established by the lifetime measurements. The solid curve represents theoretical predictions from projected shell-model calculations.

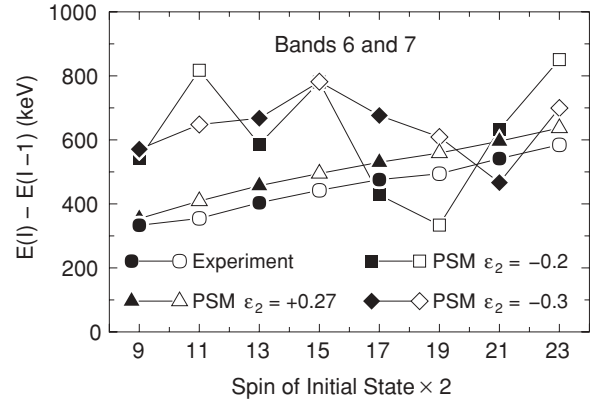

FIG. 8. Energy differences between adjacent spin states in bands 6 and 7 in ^{71}As, determined experimentally (circles) and theoretically using projected shell-model calculations assuming a prolate deformation of $\epsilon_2 = +0.27$ (triangles), and oblate deformations of $\epsilon_2 = -0.2$ (squares) and -0.3 (diamonds). Filled (open) symbols indicate states with spin I associated with a signature $\alpha = +\frac{1}{2}$ $(-\frac{1}{2})$ sequence. The experimental results assume a $\frac{7}{2}^-$ band head at an excitation energy of 1729.0 keV.

compares the PSM results with those inferred from the lifetime measurements performed in this work. Although the quantitative agreement is not nearly as good as it was for the intraband $B(E2)$ values, the qualitative trends appear to be well represented by the calculations. Any comparisons between the experimental and theoretical results should be interpreted with caution, though, since the experimental values assume a mixing ratio of $\delta = 0$.

Additional evidence for the underlying $\pi f_{7/2}$ intrinsic structure of bands 6 and 7 comes from a comparison of the measured excitation energies of states in these bands with those predicted by the PSM calculations, illustrated in Fig. 8 by the energy differences between adjacent spin states as a function of initial-state spin. As indicated in the figure, the measured energy differences show a nearly constant slope with spin, indicative of the slowly increasing $M1$ transition energies between the signature-partner bands (i.e., little or no signature splitting). This pattern is reproduced very well by the PSM calculations if a constant prolate deformation of $\epsilon_2 = +0.27$ is used (see Fig. 8), consistent with the picture of a band built on the $\pi[303]\frac{7}{2}^-$ state at large prolate deformation.

An alternative interpretation of bands 6 and 7 could involve a $\pi[303]\frac{5}{2}^-$ intrinsic configuration, since this orbital approaches the $Z = 33$ Fermi surface for small oblate deformations ($\beta_2 \approx -0.1$) [1]. In order to explore this possibility, PSM calculations of the energy differences were performed assuming quasiproton occupation of the $f_{5/2}$ orbital with a varying oblate basis deformation. Figure 8 shows the results of these calculations for two oblate basis deformations ($\epsilon_2 = -0.2$ and -0.3) that best represent the range of magnitudes inferred from the lifetime measurements in these bands. As illustrated in the figure, the results are clearly inconsistent with the experimental values, showing a rather pronounced alternating pattern (indicative of signature splitting) at low spin followed by irregularities at high spin due to the predicted onset of a band crossing. Thus the $\pi[303]\frac{5}{2}^-$ configuration appears unlikely for bands 6 and 7 based on the results of the PSM calculations. An additional argument against a $\pi[303]\frac{5}{2}^-$ intrinsic configuration is that $g_K \approx g_R$ for this orbital [3], resulting in $B(M1)$ values that should be much smaller than those measured in this work and those predicted by the PSM. Moreover, no evidence was found for a lower-lying $\frac{5}{2}^-$ state that could serve as a $K = 5/2$ band head for this structure despite a thorough search for such a state using the coincidence data.

C. Cranked Woods-Saxon calculations for bands 6 and 7

The evolution of shape and deformation with rotational frequency has been studied previously [2] for bands 1, 3, and 4 in ^{71}As using the CWS approach [1]. Similar calculations have been performed in this work in order to provide additional evidence for the intrinsic structural characteristics of bands 6 and 7.

The calculations generate a total Routhian surface (TRS) plot in the (β_2, γ) plane at discrete rotational frequencies, using a deformed Woods-Saxon potential and a short-range monopole pairing force [1]. At each grid point, the Routhian was minimized with respect to the hexadecapole deformation β_4.

In order to predict the degree of collectivity and deformation of bands 6 and 7 as a function of rotational frequency using this model, calculations were performed using non-yrast intrinsic configurations having negative parity. Using the quasiparticle labeling scheme of Ref. [28], where lowercase letters are used for 1-qp proton configurations, the g (h) configuration associated with signature $\alpha = -\frac{1}{2}$ $(+\frac{1}{2})$ was used as a possible candidate to represent band 6 (7). Although this choice does not represent an unambiguous assignment to the $\pi f_{7/2}$ orbital because of configuration mixing with other negative-parity orbitals, it does represent the lowest-energy 1-qp configuration

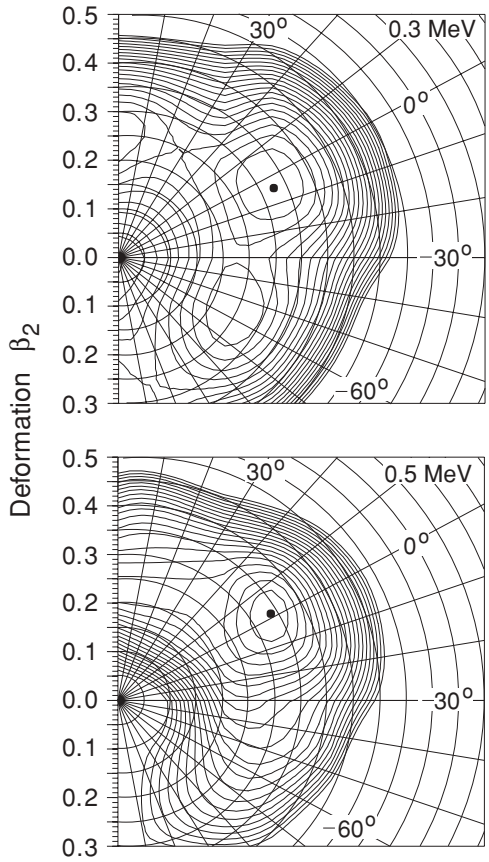

FIG. 9. Sample total Routhian surfaces in the (β_2, γ) plane for an intrinsic quasiparticle configuration that most likely represents band 7 in ^{71}As at rotational frequencies of $\hbar\omega = 0.3$ (top) and 0.5 MeV (bottom). The spacing between contour lines is 200 keV.

for non-yrast negative-parity states available in the calculations.

Figure 9 shows two representative TRS plots resulting from the calculations performed at two rotational frequencies within the range that has been observed experimentally. Although Fig. 9 only shows results for configuration h (representing band 7), very similar results were obtained at the same frequencies for configuration g (representing signature partner band 6). TRS minima with rather large quadrupole deformations approaching $\beta_2 \approx 0.35$ are indicated near the prolate-deformed axis at $\gamma = 0^\circ$ at both frequencies, indicating a near-prolate shape that remains so over the range of spins in which lifetimes were measured in this work. Using Eq. (3), the β_2 values deduced from the experimental data within bands 6 and 7 result in an average value of $|\beta_{2,\mathrm{ave}}| = 0.27(3)$, in rough agreement with the TRS calculations.

Theoretical Q_t values were calculated for bands 6 and 7 by using the β_2 values obtained from the TRS plots for the purpose of comparison with experimental values determined from Eq. (2). In order to make a proper comparison, the quadrupole deformation of the nuclear matter distribution derived from the TRS calculations was first related to the charge quadrupole deformation derived from the $B(E2)$ strengths [29,30]. In order to take triaxiality into account, the high-spin limit for the γ dependence of Q_t [31,32] was used to determine the

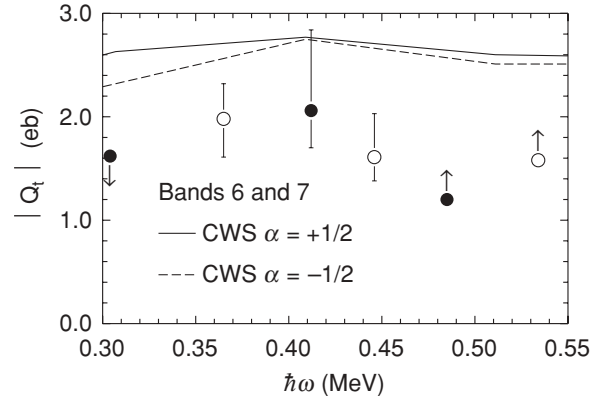

FIG. 10. Transition quadrupole moments $|Q_t|$ as a function of rotational frequency for bands 6 and 7 in ^{71}As. Filled (open) circles indicate experimental values associated with a signature $\alpha = +\frac{1}{2}$ $(-\frac{1}{2})$ sequence. Symbols with arrows indicate either upper or lower limits established by the lifetime measurements. The dashed (solid) curve represents theoretical predictions from cranked Woods-Saxon calculations for band 6 (7) with signature $\alpha = -\frac{1}{2}$ $(+\frac{1}{2})$, as indicated in the figure.

accepted theoretical Q_t values from those calculated assuming axial symmetry [29].

A comparison between the band 6 and 7 $|Q_t|$ values predicted by the CWS calculations and those obtained experimentally is shown in Fig. 10 as a function of rotational frequency. The Q_t values predicted by the CWS calculations mostly disagree with the experimental ones, with magnitudes that are systematically larger. Although one could argue that the general qualitative trends are reproduced in the calculations, there is not the same agreement with experiment as was observed between the experimental $B(E2)$ values and those calculated by the PSM (see Fig. 6). Still, the observed differences between the CWS model predictions and the experimental data do not suggest an alternative interpretation for the intrinsic structure of bands 6 and 7, especially considering that the expected near-prolate shape associated with these bands has been confirmed by the TRS calculations.

V. SUMMARY

High-spin states in ^{71}As were studied using the ^{54}Fe(^{23}Na,$\alpha 2p$) reaction at 80 MeV performed at the John D. Fox superconducting accelerator at Florida State University. The isotopically enriched ^{54}Fe target was thick enough to stop all recoils and hence allowed for the measurement of lifetimes using the Doppler-shift attenuation method (DSAM). γ rays were detected in prompt coincidence using a Compton-suppressed Ge array consisting of three high-efficiency clover detectors and seven single-crystal detectors. The existing high-spin level scheme of ^{71}As has been confirmed, and 21 new transitions have been added based on the investigation of weak γ-γ coincidence relationships. The lifetimes of 16 excited states were measured using the DSAM, with the experimental line shapes obtained at two separate detector angles and by gating from above the transitions of interest whenever possible.

Lifetimes were measured for the first time in the bands suggested to be based on the $\pi[303]\frac{7}{2}^-$ configuration at prolate deformation. This interpretation appears to be confirmed in this work, as the predicted behavior of the $B(E2)$ and $B(M1)$ rates and the $M1$ transition energies with spin from projected shell-model (PSM) calculations assuming this configuration show good overall agreement with the experimental results. On the other hand, the predicted $M1$ transition energies assuming a $\pi[303]\frac{5}{2}^-$ configuration at oblate deformation do not reproduce the measured trend with spin. Total Routhian surfaces resulting from cranked Woods-Saxon calculations for non-yrast negative-parity configurations point to a strongly deformed, near-prolate shape for this structure, providing further evidence in favor of the existing interpretation.

Two new lifetimes were measured in the yrast positive-parity band, which was extended up to a $(\frac{33}{2}^+)$ state. No new evidence was found for the onset of the first quasineutron alignment in this structure. The qualitative features of the $B(E2)$ strengths in this band are roughly followed by the PSM calculated values.

Two new mean lifetimes were measured in the lowest negative-parity bands, while upper or lower limits were set on four other states. The $B(E2)$ values for these sequences are generally in poor agreement with the PSM predictions, evidently indicating the need to account for triaxiality in the calculations.

Of the new γ-ray transitions that were found, some were organized to form two bands that decay to the yrast negative-parity bands, and others established links between some of the high-spin negative-parity bands and low-lying negative-parity states known from EC + β^+ decay. A new state at 1467.8 keV was observed and interpreted as the band head of the unfavored sequence of yrast negative-parity states. Similarly, the known $\frac{5}{2}^-$ state at 1245.5 keV may be the lowest-lying member of the favored signature partner band.

ACKNOWLEDGMENTS

This work was supported in part by the US National Science Foundation through Grants No. PHY-04-56463 (FSU) and No. PHY-0648751 (OWU), as well as the Ohio Wesleyan University Summer Science Research Program. Research at Shanghai Jiao Tong University was supported by the Shanghai Pu-Jiang program, the National Natural Science Foundation of China under Contract No. 10875077, the Doctoral Program of High Education Science Foundation under Grant No. 20090073110061, and the Chinese Major State Basic Research Development Program under Grant No. 2007CB815005. We thank W. Nazarewicz for providing the results of his cranked Woods-Saxon calculations, and the staff of the FSU John D. Fox superconducting accelerator for their support throughout the experiment.

[1] W. Nazarewicz, J. Dudek, R. Bengtsson, T. Bengtsson, and I. Ragnarsson, Nucl. Phys. A **435**, 397 (1985).
[2] R. S. Zighelboim, S. G. Buccino, F. E. Durham, J. Döring, P. D. Cottle, J. W. Holcomb, T. D. Johnson, S. L. Tabor, and P. C. Womble, Phys. Rev. C **50**, 716 (1994).
[3] N. Fotiades *et al.*, Phys. Rev. C **59**, 2919 (1999).
[4] H. Toki and A. Faessler, Phys. Lett. B **63**, 121 (1976).
[5] B. Heits, H.-G. Friederichs, A. Gelberg, K. P. Lieb, A. Perego, R. Rascher, K. O. Zell, and P. von Brentano, Phys. Lett. B **61**, 33 (1976).
[6] G. M. Gusinskii, V. S. Zvonov, I. Kh. Lemberg, and V. E. Mitroshin, Izv. Akad. Nauk SSSR, Ser. Fiz. **44**, 92 (1980).
[7] C. E. Svensson *et al.*, Phys. Rev. Lett. **79**, 1233 (1997).
[8] C. E. Svensson *et al.*, Phys. Rev. Lett. **80**, 2558 (1998).
[9] I. Stefanescu *et al.*, Phys. Rev. C **70**, 044304 (2004).
[10] B. O. Ten Brink, P. van Nes, C. Hoetmer, and H. Verheul, Nucl. Phys. A **338**, 24 (1980).
[11] J. Pavan, Ph. D. thesis, Florida State University, 2003.
[12] [http://fsunuc.physics.fsu.edu/~caussyn/].
[13] P. Petkov, D. Tonev, J. Gableske, A. Dewald, and P. von Brentano, Nucl. Instrum. Methods Phys. Res., Sect. A **437**, 274 (1999).
[14] F. Brandolini and R. V. Ribas, Nucl. Instrum. Methods Phys. Res., Sect. A **417**, 150 (1998).
[15] P. Petkov, D. Tonev, A. Dewald, and P. von Brentano, Nucl. Instrum. Methods Phys. Res. Sect. A **488**, 555 (2002).
[16] E. F. Moore, P. D. Cottle, C. J. Gross, D. M. Headly, U. J. Hüttmeier, S. L. Tabor, and W. Nazarewicz, Phys. Rev. C **38**, 696 (1988).
[17] [http://www.srim.org].
[18] R. A. Kaye *et al.*, Phys. Rev. C **69**, 064314 (2004).
[19] F. Cristancho and K. P. Lieb, Nucl. Phys. A **486**, 353 (1988).
[20] S. L. Tabor, J. Döring, J. W. Holcomb, G. D. Johns, T. D. Johnson, T. J. Petters, M. A. Riley, and P. C. Womble, Phys. Rev. C **49**, 730 (1994).
[21] F. Cristancho *et al.*, Nucl. Phys. A **501**, 118 (1989).
[22] K. Hara and Y. Sun, Int. J. Mod. Phys. E **4**, 637 (1995).
[23] R. Palit, J. A. Sheikh, Y. Sun, and H. C. Jain, Nucl. Phys. A **686**, 141 (2001).
[24] R. Palit, J. A. Sheikh, Y. Sun, and H. C. Jain, Phys. Rev. C **67**, 014321 (2003).
[25] Y. Sun, Eur. Phys. J. A **20**, 133 (2004).
[26] R. A. Kaye *et al.*, Phys. Rev. C **75**, 034311 (2007).
[27] Y. Sun and J. L. Egido, Nucl. Phys. A **580**, 1 (1994).
[28] R. Wyss, F. Lidén, J. Nyberg, A. Johnson, D. J. G. Love, A. H. Nelson, D. W. Banes, J. Simpson, A. Kirwan, and R. Bengtsson, Nucl. Phys. A **503**, 244 (1989).
[29] W. Nazarewicz, M. A. Riley, and J. D. Garrett, Nucl. Phys. A **512**, 61 (1990).
[30] J. Dudek, W. Nazarewicz, and P. Olanders, Nucl. Phys. A **420**, 285 (1984).
[31] I. Hamamoto and B. R. Mottelson, Phys. Lett. B **132**, 7 (1983).
[32] P. Ring, A. Hayashi, K. Hara, H. Emling, and E. Grosse, Phys. Lett. B **110**, 423 (1982).